The effect of dendritic spine morphology on synaptic crosstalk

A multisynapse model, integrating diffusion on curved surfaces

Tamara Kloek

Technische Universiteit Delft

TU Delft Delft University of Technology

Challenge the future

THE EFFECT OF DENDRITIC SPINE MORPHOLOGY ON SYNAPTIC CROSSTALK

A MULTISYNAPSE MODEL, INTEGRATING DIFFUSION ON CURVED SURFACES

by

Tamara Kloek

in partial fulfillment of the requirements for the degree of

Master of Science

in Applied Mathematics

at the Delft University of Technology,

to be defended publicly on Thursday June 4, 2015 at 11:00 AM.

Supervisor:	Dr. ir. F. J. Vermolen,	TU Delft
	Ir. R. P. T. Kusters,	TU Eindhoven
Thesis committee:	Dr. ir. F. J. Vermolen,	TU Delft
	Prof. dr. ir. C. Vuik,	TU Delft
	Dr. ir. J. L. A. Dubbeldam,	TU Delft

This thesis is confidential and cannot be made public until June 4, 2015.

TU Delft Delft University of Technology

CONTENTS

1

INTRODUCTION: DENDRITIC SPINES AND THEIR ROLE IN THE NERVOUS SYSTEM

1.1. THE NERVOUS SYSTEM

The nervous system is the organ system of the body that coordinates both conscious as well as unconscious actions and transmits signals between different parts of the body. The control of muscles, processing sensory stimuli and regulating cognitive processes are all carried out by the nervous system. In most animal bodies the nervous system consists of two main parts, the central nervous system (CNS) and the peripheral nervous system. The first one consists of the brain and the spinal cord and the latter one connects the central nervous system to every other part of the body.

At the cellular level the nervous system consists of a special type of cells, called neurons or nerve cells. Their structure allows them to transmit signals fast and effectively to other cells. Internally signals are sent in the form of electrochemical waves along thin fibers of the cell itself. Between different cells these signals are mainly transmitted through specialized junctions called synapses.

1.1.1. NEURONS

Neurons or nerve cells are the cells that constitute the nervous system. They are characterized by a specific composition that allows them to transmit signals from and to every part of the body. Specialized type of neurons are designed to perform a specific task and include:

- *Sensory neurons* are sensitive to input from outside the body like touch, sound, light, smell and other types of external stimuli. After receiving such stimuli they transmit signals to the central nervous system.
- *Motor neurons* are able to directly or indirectly control muscles or glands after receiving input from the central nervous system.
- *Interneurons* connect neurons to other neurons and are mainly found in the central nervous system.

A typical schematic graphic of the structure of two interconnected neurons can be found in figure 1.1. Neurons are highly specialized for the processing and transmission of signals and this is reflected in their anatomy. A typical neuron possesses a cell body or soma, multiple dendrites, an axon and an axon terminal.

- The *soma* is the cell body of the neuron. It contains the nucleus, where most of the cell's genetic material is located. The nucleus of a neuron is involved in processing signals and determining whether a signal is to be transmitted or inhibited.

- *Dendrites* are thin structures that arise from the cell body and often branch multiple times forming a typical dendritic tree. This collection of dendritic protrusions is where the majority of input to the neuron occurs. They receive input from other neurons and propagate the signal to the cell body.
- An *axon* is a structure that arises from the cell body and carries nerve signals away from the soma to other nerve cells or different parts of the nervous system. Whereas a nerve cell has multiple dendrites it typically possesses only one axon. Compared to dendrites an axon can be very long and signals travel the majority of their distance via axons.
- The *axon terminal* is formed when the axon undergoes extensive branching at its end. It contains the synaptic terminals, where neurotransmitter chemicals are released to communicate with target neurons.

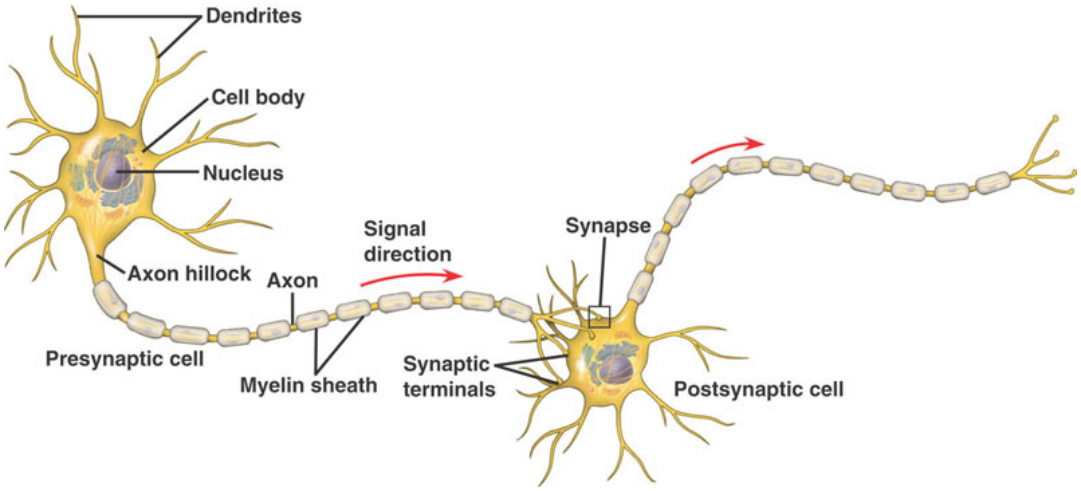

Figure 1.1: Structure of two interconnected neurons. Image: shutterstock.

1.1.2. SYNAPSES

A synapse is a structure where the signal transmission between two neurons occurs. There are two fundamentally different types of synapses: chemical synapses and electrical synapes. In electrical synapses an electronic signal is transmitted by special channels connected to the presynaptic membrane on the one side and to the postsynaptic membrane on the other side.

In this research, we shall focus on chemical synapses. In chemical synapses the transmitting neuron releases a chemical substance, called neurotransmitter, in the synapse which can bind to a corresponding cell surface receptor on the receiving cell. This cell may then be excited, inhibited or otherwise modulated. Chemical synapses can be subdivided again into two main categories: excitatory and inhibitory synapses. An excitatory synapse is a type of synapse in which an action potential in the presynaptic neuron increases the probability of an action potential occurring in the postsynaptic cell. This is in contrast to inhibitory synapses, which have – as the name suggests – an inhibitory effect on the activation of the postsynaptic neuron. When excitatory effects exceed those of inhibitory effects, the receiving neuron will fire an action potential and thereby information is transferred between the involved neurons. Next, we will focus on excitatory synapses.

ANATOMY AND FUNCTION OF EXCITATORY SYNAPSES

An excitatory synapse is a synapse in which an action potential in the presynaptic neuron increases the probability of an action potential occuring in the postsynaptic cell. They have a fundamental role in information processing within the CNS. Knowing the typical anatomy of synapses is crucial in understanding their function. In figure 1.2 a schematic overview of the anatomy of an excitatory synapse is displayed. We shall discuss the components shown.

In the presynaptic specialization lies a cluster of synaptic vesicles containing neurotransmitter close to the

presynaptic cell membrane, which we call the active zone. Exocytosis of these vesicles releases neurotransmitter in the synaptic cleft. An elaborated review of the presynaptic specialization and the synaptic vesicle cycle can be found in [1].

The essential postsynaptic components of an excitatory synapse are located on the dendritic spine, which we shall discuss in more detail later on. A detailed review of the architecture of the postsynaptic specialization of excitatory synapses can be found in [2]. Opposed to the active zone, on the postsynaptic membrane lies its counterpart, a protein dense regime called the postsynaptic density (PSD). The PSD contains scaffold proteins, which are known to interact with neurotransmitter receptors, thus binding them to the PSD. At the PSD neurotransmitter receptors, like AMPA and NMDA receptors , are highly concentrated. The presence of a PSD is characteristic for excitatory synapses, inhibitory synapses lack such a thickening in the postsynaptic cell membrane. The rest of the postsynaptic membrane can be divided into perisynaptic (close to the synapse) and extrasynaptic (outside the synapse) regions. The active zone and the PSD are separated by a gap called the synaptic cleft.

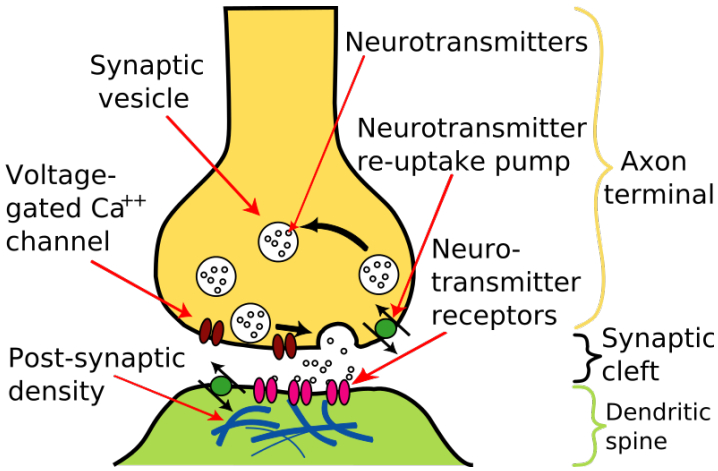

Figure 1.2: Anatomy of an excitatory synapse. CC BY-SA 3.0. Original in [3].

1.1.3. DENDRITIC SPINES

The dendrite of a neuron receives signals from other neurons. Most of the excitatory inputs are located on dendritic spines. Spines are protrusions of the membrane of the postsynaptic cell, on which the PSD is located. They consist of a spine head and a thin spine neck which connects them to the dendritic shaft (figure 1.3). A high correlation is found between the dimensions of spines and the size of the PSD [4, 5]. The shape of spines can be described as “thin”, “stubby” or “mushroom”. The dendritic spine is a dynamic structure, whose shape, size and composition change during development and in response to synaptic activity [6, 7]. Changes in their size and shape are connected with a change in synaptic strength.

The relation between morphology and function is a central theme within biology. The way that the nontrivial morphology of dendritic spines influence their function is not yet fully understood. Having structures like spines containing synapses along the dendrite may have several advantages. Evidently, spines might assist in signaling by physically forming a bridge from axon to dendrite [9]. However, not all synapses are constituted by spines and dendrites can receive inputs directly on their shafts. It is therefore likely that spines are also beneficial in another way. It has been widely suggested that they are associated with compartmentalization, enabling the different synapses to work as independent components [8] . “Mushroom” spines typically have a bulbous head (spine head) and are connected with their corresponding dendrite through a thin spine neck. This morphology allows spines to serve as compartments by which one synapse can be isolated from other synapses on the same neuron.

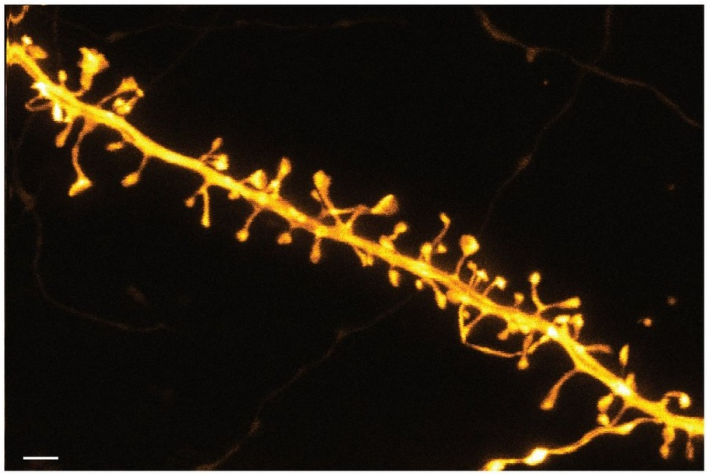

Figure 1.3: STED image recorded from a living dendrite including spines. Source: [8].

1.2. SYNAPTIC PLASTICITY

Synaptic plasticity is the ability of synapses to strengthen and weaken over time, in response to a change in their activity. If this strengthening and weakening persists, then long-lasting increase or decrease in synaptic strength occurs, which is called long-term potentiation (LTP) and long-term depression (LTD) respectively.

Since memories are postulated as networks of neurons in the brain, altering synaptic strength is thought to be one of the most important mechanisms that constitute memory and learning. Synaptic transmission of signals and synaptic plasticity are crucial for proper functioning of the central nervous system. Failure of these mechanisms are associated with many neurological and neuropsychiatric disorders like schizophrenia, Alzheimer disease, depression and autism [10, 11]. Furthermore, plasticity of synapses located in the brain (brain plasticity) is thought to play an important role in stroke rehabilitation [12]. Therefore, it is of clinical importance to gain a better understanding of the mechanism that influence synaptic plasticity.

The strength of synaptic transmission between neurons can be modified by various factors, like the density of neurotransmitter receptors located on the postsynaptic neuron [13] and the quantity of neurotransmitters released into the synapse [14]. If the amount of neurotransmitter released into the synapse exceeds a certain threshold in concentration that saturates the postsynaptic receptors, then the number of available and properly functioning receptors will be the most important limiting factor [14, 15]. Controlling the number of receptors at excitatory synapses is of fundamental importance in synaptic transmission [16]. It is therefore of great importance to understand the mechanisms behind receptor trafficking in dendrites and more specifically in dendritic spines.

1.2.1. RECEPTOR TRAFFICKING AT SYNAPSES

We know that the phenomena of synaptic plasticity depends strongly on the density of neurotransmitter receptors at the PSD of the postsynaptic cell. Therefore it is interesting to investigate the factors that influence this density. Three main mechanisms that drive the receptor traffic can be distinguished.

The first mechanism is endocytosis and exocytosis of receptors from intracellular vesicles. These are energy-consuming processes in which receptors are transported from the cell membrane into the intracellular space (endocytosis) or the other way around (exocytosis).

Second, anchoring of receptors at the PSD has been the focus of numerous studies. The PSD partially consists of scaffold proteins, which are known to bind to the receptors. This mechanism ensures trapping of receptors at the site of the PSD.

The third mechanism controlling receptor trafficking at synapses is surface diffusion. In general, receptors are not bound to the cell membrane, but can diffuse freely until being transported to the intracellular space (endocytosis) or anchored at scaffold proteins (for example at the PSD).

A factor influencing how these mechanisms work is the morphology of the dendritic spine on which the synapse is located [17]. The morphology of a spine is nontrivial. The necessity of having this shape and the function of spines are not well understood. Since it is widely accepted that changes of structure of the brain are caused by changes of activity of the brain, research has focused on the implications of nontrivial morphological structures [5–7, 17, 18].

1.2.2. SYNAPTIC CROSSTALK

Crosstalk between synapses refers to instances in which components from one synapse influences the signal transmission in other synapses. An example is when a summation of neurotransmitter released in a synapse creates a spill-over to other synapses and thereby creates extrasynaptic signaling. For specific signaling, it is important that synapses can be strengthened and weakened individually in response to their specific activity (synaptic plasticity). Synaptic crosstalk undermines the ability of the body to specifically control the strength of individual synapses.

Since receptors can diffuse across the cell membrane, they can also be a cause of synaptic crosstalk. An important question is how an exocytic event in one synapse affects the amount of receptors in neighboring synapses. In other words, if receptors are released in one spine, what kind of implications does this have on the concentration of receptors in neighboring spines. We would like to investigate the influence of the morphology of dendritic spines on this synaptic crosstalk. A model concerning this question does not exist yet. The morphology of spines is thought to cause compartmentalization enabling excitatory synapses to function as individual components and we would like to explore to what extent.

1.3. RESEARCH QUESTIONS

After this introduction to dendritic spines and their role in the nervous system, we can formulate our research question:

> How does the morphology of dendritic spines influence the synaptic crosstalk?

The subquestions belonging to this main research question are:

> How should the morphology of dendritic spines be defined?
> What constitutes a good comparison between shapes?
> What is a measure for the amount of synaptic crosstalk?

As shall be discussed in Chapter 2 a model considering more than one synapse (multisynapse models) that integrates the nontrivial three-dimensional morphology that typifies dendritic spines does not exist. Therefore the influence of the shape of these dendritic spines on their interaction is not yet addressed.

2

EXISTING MODELS FOR SYNAPTIC RECEPTOR TRAFFICKING

In this section we explore the existing models for synaptic receptor trafficking. We distinguish single synapse and multisynapse models and furthermore make a subdivision based on how these models deal with the geometry of synapses. Furthermore we shall give an overview of the methods used per model.

2.1. SINGLE SYNAPSE MODELS

As the name suggests single synapse models model the synaptic receptor trafficking considering one synapse. They typically investigate the mean first passage time (MFPT) from the top of the synapse to the dendrite and the residence time of receptors at the postsynaptic density. A variety of models exist and they have a different approach both in the aspect of modeling receptor trafficking, trapping and recycling as well as the aspect of geometry of the domain.

2.1.1. HOLCMAN AND SCHUSS, 2011

Holcman and Schuss [19] took the nontrivial geometry into account and defined a domain of computation that incorporated the relatively large head and narrow neck. They use analytical methods to compute the mean first passage time from spinelike structures. More specifically, they study the residence time of a Brownian particle from the spine head to an absorbing boundary at the end of the spine neck. These particles move either on a two-dimensional (flat) or inside a three-dimensional domain. The two- and three-dimensional composite domains Ω considered consist of a head, Ω_1, connected through a small interface $\partial\Omega_i$ to a narrow cylindrical neck Ω_2 as shown in figure 2.1. The two-dimensional domain is a cross section of the three-dimensional domain. The boundary of Ω is reflecting, except the far end of domain Ω_2. Furthermore they distinguish between a bottleneck connected by a smooth funnel to the neck and a nonsmooth connection between head and neck as in figure 2.1.

Holcman and Schuss compute the MFPT as proposed in [20] and consider a Brownian motion $\boldsymbol{x}(t)$. The expected lifetime of $\boldsymbol{x}(t)$ in Ω, given $\boldsymbol{x}(0) = \boldsymbol{x} \in \Omega$, is the MFPT $v(\boldsymbol{x})$ of $\boldsymbol{x}(t)$ from $\boldsymbol{x}$ to $\partial\Omega_a$ and the solution of the mixed boundary value problem

$$\Delta v(\boldsymbol{x}) = -\frac{1}{D} \quad \text{for} \quad \boldsymbol{x} \in \Omega \tag{2.1}$$

$$v(\boldsymbol{x}) = 0 \quad \text{for} \quad \boldsymbol{x} \in \partial\Omega_a \tag{2.2}$$

$$\frac{\partial v(\boldsymbol{x})}{\partial n} = 0 \quad \text{for} \quad \boldsymbol{x} \in \partial\Omega_r, \tag{2.3}$$

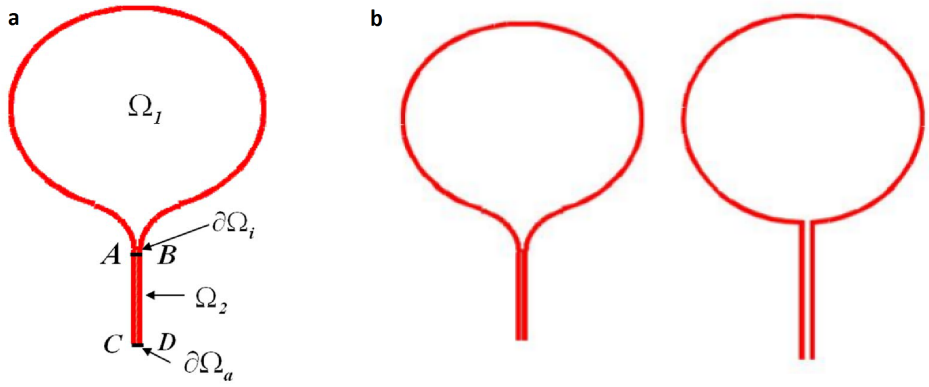

Figure 2.1: (a) The composite domain consist as used by [19]. The entire boundary is reflecting ($\partial\Omega_r$, in red), except for a small absorbing part $\partial\Omega_a$. (b) A cross section of a nonsharp and sharp connection.

where D denotes the diffusion constant, $\partial\Omega_r$ denotes the reflecting boundary and $\frac{\partial v(\boldsymbol{x})}{\partial n}$ is the directional derivative taken in the direction normal to the boundary at point $\boldsymbol{x}$. If the size of the absorbing part $\partial\Omega_a$ is sufficiently smaller than the reflecting part $\partial\Omega_r$, it can be shown that the MFPT is to leading order independent of $\boldsymbol{x} \in \Omega$.

Both the MFPT from the head to the interface connecting the head and the neck, $\overline{\tau}_{\boldsymbol{x}\to\partial\Omega_i}$ and the MFPT from this interface to the absorbing boundary, $\overline{\tau}_{\partial\Omega_i\to\partial\Omega_a}$ are computed. The MFPT from the head to the absorbing boundary can then be represented as

$$\overline{\tau}_{\boldsymbol{x}\to\partial\Omega_a} = \overline{\tau}_{\boldsymbol{x}\to\partial\Omega_i} + \overline{\tau}_{\partial\Omega_i\to\partial\Omega_a}. \tag{2.4}$$

$\overline{\tau}_{\partial\Omega_i\to\partial\Omega_a}$ is harder to calculate, since both $\partial\Omega_i$ and $\partial\Omega_a$ are boundaries of domain Ω_2. See [20] for further details on this computation.

The presented results include the relation between neck radius and neck length and MFPT. The geometry of the connection (smooth or nonsmooth) affects this relationship significantly and to a larger extent in the two-dimensional than in the three-dimensional case.

DISCUSSION

The method that Holcman and Schuss present is elegant and allows an analytical representation for calculation of the MFPT. The derivation of this representation, however, is based on heavy assumptions on the geometry. For example, for diffusion on the surface of the three-dimensional domain the head is assumed to be spherical. This model considers only MFPT from the head of the spine to the exit of the spine (to the dendrite) and cannot be used for trapping at the PSD by assuming an absorbing boundary there, because of assumptions on the geometry. For more complex geometries numerical methods have to be used. Therewithal the model considers a system of one synapse and therefore cannot be used or has to be heavily adjusted to investigate the synaptic crosstalk between multiple synapses.

2.1.2. KUSTERS ET AL., 2013

Kusters et al. [21, 22] incorporated curved geometries in their work as well. They combined random walk simulations with calculations of mean first passage times to study the diffusive time scales and escape rates for different geometrical properties of the domain of computation. They consider lateral diffusion on an axisymmetric curved surface. The domain consist of a bulbous head and a funnellike neck and is parameterized as

$$\boldsymbol{r}(u,\theta) = \begin{pmatrix} R\sin u\cos\theta \\ R\sin u\sin\theta \\ h - \frac{R\cos u}{Au} \end{pmatrix}, \tag{2.5}$$

where R is the maximal radial distance of the surface, h a measure for the height of the funnel, and A a shape parameter which is large for systems with a narrow neck and small for systems with a wider neck. T. For $R = 1$ and $h = 4$ the influence of A is shown in figure 2.2.

Figure 2.2: Influence of A on shape as parametrized by [21].

The in-plane Brownian motion of the particles on a curved surface is simulated using a method extensively discussed in [23]. Briefly, the random walk is produced as trajectories of fixed length steps in random directions on a curved geometry with in-plane coordinates u and θ. On a curved surface both selecting a random direction and traveling a fixed distance require some attention. A random directional unit vector $\overrightarrow{w}$ is of unit length when we subject it to the constraint $g_{uu}(w^u)^2 + g_{\theta\theta}(w^\theta)^2 = 1$, where g_{ij} are entries of the metric. Note that for axisymmetrical surfaces $g_{ij} = 0$ when $i \neq j$.

Next, a geodesic curve in the direction of $\overrightarrow{w}$ is approximated, parametrized by the arc length s, using a second order approximation of the tangential plane

$$\boldsymbol{r}(s+\mathrm{d}s) \approx \boldsymbol{r}(s) + \frac{\mathrm{d}\boldsymbol{r}(s)}{\mathrm{d}s}\mathrm{d}s + \frac{1}{2}\frac{\mathrm{d}^2\boldsymbol{r}(s)}{\mathrm{d}s^2}\mathrm{d}s^2. \tag{2.6}$$

The first derivative is simply the unit tangent vector $\overrightarrow{w}$ and the second derivative is obtained by solving the geodesic equation

$$\frac{\mathrm{d}^2\boldsymbol{r}(s)}{\mathrm{d}s^2} = -\Gamma^i_{kl}\frac{\mathrm{d}r^l}{\mathrm{d}s}\frac{\mathrm{d}r^k}{\mathrm{d}s}. \tag{2.7}$$

If a step size λ is used, this method results in a shift in coordinates for every iteration given by

$$\Delta u = w^u\lambda - \frac{1}{2}\Gamma^u_{uu}(w^u)^2\lambda^2 - \Gamma^u_{u\theta}w^u w^\theta\lambda^2 - \frac{1}{2}\Gamma^u_{\theta\theta}(w^\theta)^2\lambda^2, \tag{2.8}$$

$$\Delta\theta = w^\theta\lambda - \frac{1}{2}\Gamma^\theta_{uu}(w^u)^2\lambda^2 - \Gamma^\theta_{u\theta}w^u w^\theta\lambda^2 - \frac{1}{2}\Gamma^\theta_{\theta\theta}(w^\theta)^2\lambda^2. \tag{2.9}$$

This method leads to trajectories that are locally Brownian to second order in curvature. An extensive discussion of this method in general can be found in [23] and an application to this problem can be found in [22].

Kusters et al. also calculate the MFPT. They do so using almost the same mixed boundary value problem as [19]. A small modification is made however, Eq. (2.1) is substituted by

$$\nabla^2 W = -\frac{1}{D}, \tag{2.10}$$

where D is the diffusion constant, W is the MFPT and ∇^2 is the Laplace-Beltrami operator, which can be calculated using the metric and Christoffel symbols. The more general Laplace-Beltrami operator is used to account for the curvature of the domain. With this substitution the calculation of the MFPT is equivalent for both methods.

They find a general power law dependence for both the equilibrium time scale of a population of particles and a single-particle characteristic time of escape time. The equilibrium time τ_{eq} depends on neck radius and neck length by the general relations

$$\tau_{eq} = (\text{neck radius})^{-\alpha}, \quad \alpha > 0 \tag{2.11}$$

$$\tau_{eq} = (\text{neck length})^{\beta}, \quad \beta > 0. \tag{2.12}$$

α and β are some positive constants and their exact value depends on the specific geometry.

DISCUSSION

The random walk method used by Kusters et al. [21, 22] is very flexible in terms of types of geometries it can be used with. As long as the metric and Christoffel symbols of the surface are available this method can be applied. In order to compute the metric and Christoffel symbols, it should be possible to calculate or (numerically) approximate first and second derivatives of the parametrization of the surface. So, we only require sufficiently smooth surfaces to apply this method.

Analytical calculation of the MFPT using Eq. (2.10) can be used to compare stochastic simulation results to. Therefore it can be used as a benchmark for the simulation results.

The model presented by Kusters et al. [21, 22] focuses on one spine only. Therefore interactions between spines cannot be studied. The model is, however, suitable to be extended to a multisynapse model.

2.2. MULTISYNAPSE MODELS ON SIMPLE TWO-DIMENSIONAL GEOMETRIES

The multisynapse models that exist model dendrites as simple shapes, like flat or cylindrical surfaces. Synapses are modeled as components coinciding with the surface of the dendrite. The nontrivial shape of spines is reflected in different diffusive properties on these components, but is not explicitly taken into account. Here, we shall discuss some of these models.

2.2.1. CZÖNDÖR ET AL., 2012

Czöndör et al., [24], propose a model that uses random walk simulation on a flat surface. The model takes the three major mechanisms of receptor trafficking into account: surface diffusion, anchoring at the postsynaptic density and endo/exocytic recycling of receptors. They define a flat working space, we shall call Ω, of length L and width w with rebound conditions on each side. Postsynaptic spines are modeled as square obstacles with lower diffusion constant and each synapse contains a square PSD which allows trapping. Also exocytic and endocytic events were introduced.

Surface diffusion was modeled by updating the positions $x(t)$ and $y(t)$ of a particle each time step by incrementing them by $\sqrt{2D\Delta t}Z_x$ and $\sqrt{2D\Delta t}Z_y$ respectively, were Z_x and Z_y are realizations of a standard normal

distribution. This comes down to a simple application of the Euler method to the stochastic differential equation

$$\mathrm{d}\boldsymbol{X}_t = \sqrt{2D}\,\mathrm{d}\boldsymbol{W}_t, \tag{2.13}$$

where $\boldsymbol{W}_t$ is a Wiener process. This represents two-dimensional diffusion of a single particle with constant diffusion coefficient D and without convection. The mean squared displacement for each time step and each particle is therefore $\mathbb{E}[||\boldsymbol{X}_{t+\Delta t} - \boldsymbol{X}_t||] = 4D\Delta t$. The corresponding diffusion equation is the two-dimensional diffusion equation with constant diffusion coefficient D and no convection

$$\frac{\partial c(\boldsymbol{r},t)}{\partial t} - D\Delta c(\boldsymbol{r},t) = 0, \quad \boldsymbol{r} \in \Omega. \tag{2.14}$$

If a receptor reached a postsynaptic area, it was set to diffuse with a lower diffusion coefficient. The simulation method remains otherwise the same. Whenever a receptor reached a PSD area, binding to the PSD was modeled by a random variable with a bernoulli distribution with succes probability proportional to the time step Δt and a certain predefined rate k_{on}. During binding the receptor was set to diffuse with an even lower diffusion coefficient, furthermore detachment was modeled using a random variable with bernoulli distribution with succes probability proportional to the time step, but with a possible different rate, k_{off}, than for binding.

To mimic exocytic events, new trajectories were initiated. Here, the number of receptors, exocytic site, timing and frequency of an exocytosis were specified.

To simulate endocytic events square endocytic zones (EZs) were introduced. The event of absorption is thereafter modeled in the same way as anchoring at the PSD, by a random variable with a Bernoulli distribution with success probability proportional to the time step and a certain predefined rate k_{endo}.

Czöndör et al. present results of their simulation in which they consider the influence of (extra)synaptic endo/exocytic events on the receptor concentration in surrounding synapse(s). Furthermore, the outputs of the simulation are directly comparable to single particle tracking (SPT) and fluorescence recovery after photobleaching (FRAP) experiments and can therefore be easily benchmarked.

DISCUSSION

The work of Czöndör et al. in [24] incorporates the three major mechanisms influencing synaptic receptor trafficking. It is very useful that their results are directly comparable to SPT and FRAP data.

They model synapses as flat surfaces which is not the typical shape of spines belonging to excitatory synapses. However, the way trapping is modeled here can be integrated in a model that incorporates the typical three-dimensional shape. Furthermore, even though the model allows for integration of multiple synapses, they do not regard the synaptic crosstalk.

2.2.2. BRESSLOFF ET AL., 2008

Bressloff et al. [25] proposed a model in which they model a dendrite as a two-dimensional cylindrical surface with small, partially absorbing holes, which represent the transverse intersections of the spines with the dendrite. In [25], they present an extension of their work in [26] where a model of receptor trafficking at a single dendritic spine is treated.

They formulate a diffusion-trapping model on a cylinder with length L and radius l. They neglect the extrinsic curvature of the membrane because protein receptors and spine necks are much smaller than the circumference of the cylinder. Therefore, they represent their surface as a long rectangular domain Ω_0,

$$\Omega_0 = \{(x,y) : 0 < x < L, |y| < \pi l\}. \tag{2.15}$$

Here, x is the coordinate in the direction of the axis of the cylinder and y is the coordinate in the radial direction of the cylinder. At $x = 0$ they impose a nonzero flux boundary condition, which represent a constant inflow of of new receptors. On the other end, at $x = L$, they impose a no-flux boundary condition, modeling a reflecting boundary. On $y = \pm\pi l$ they impose periodic boundary conditions,

$$c(t,(x,\pi l)) = c(t,(x,-\pi l)) \tag{2.16}$$
$$\frac{\partial c}{\partial y}(t,(x,\pi l)) = \frac{\partial c}{\partial y}(t,(x,-\pi l)) \tag{2.17}$$

Each spine neck is modeled as a circular intersection with radius ϵ, Ω_j, where j labels the j^{th} spine. The surface of the cylinder excluding these small discs is denoted by $\Omega_\epsilon = \Omega_0 \setminus \cup_{j=1}^{N} \Omega_j$. Because of the small area of each spine, they assume the receptor concentration within each spine to be spatially homogeneous and equal to $\tilde{c}_j$ for spine j. The dendritic surface receptor concentration evolves according to the diffusion equation

$$\frac{\partial c}{\partial t} = D\nabla^2 c. \tag{2.18}$$

On the boundary of each Ω_j, $\partial\Omega_j$, they impose the mixed boundary condition

$$\epsilon\partial_n c(\boldsymbol{r},t) = -\frac{\omega_j}{2\pi D}\left(c(\boldsymbol{r},t) - \tilde{c}_j\right), \quad \boldsymbol{r} \in \partial\Omega_j, \quad j = 1,\ldots,N, \tag{2.19}$$

where $\partial_n c$ is the outward normal derivative to Ω_ϵ. The physical interpretation is that the flux of receptors between a specific spine and the dendrite depends on the difference in concentration between either side of the boundary with ω_j as effective hopping rate.

A pair of differential equations determines the value of $\tilde{c}_j$ over time and concludes the model. These equations shall not be discussed here, but an extensive review of the full method can be read in [25].

An analysis of this model is done by constructing the steady-state solution using singular perturbation techniques. These results are compared with numerical solutions of the full model and with a reduced one-dimensional model.

They show that for long, thin dendrites the variation of the receptor concentration around the circumference of the dendrite is negligible so that the dendrite can be modeled a simpler one-dimensional cable. They remark that the difference between the one and two-dimensional can become significant in the case of short dendrites with few spines. Also, they note that an important extension of their work would be to consider a much more detailed model of receptor trafficking within each spine.

DISCUSSION

The paper of Bressloff et al., [25], is the most mathematical work considered. They give an extensive analysis of their model and verify their results.

This work does not investigate how (the shape of) spines influence their own concentration or the concentration in neighboring spines. Moreover, they assume a constant inflow of receptors at one side of the domain and do not explore the effect of the precise location of exocytosis.

2.2.3. OTHER MULTISYNAPSE MODELS

More multisynapse models do exist, but we will not give an extensive review of these.

Holman and Triller (2006), [27], propose a two-dimensional model in which they account for binding to scaffolding molecules in the PSD and the presence of obstacles to diffusion. They derive Markovian equation and analyze steady-state solutions. They argue that when the fluxes involve a sufficiently large number of receptors, the dynamics of the receptors can be modeled using standard differential equations of chemical reactions and a system of differential equations is proposed and analyzed. Furthermore they suggest a way to use the model to interpret FRAP data.

Earnshaw and Bressloff propose a model in [28] that is similar to their work in [25], discussed in section 2.2.2, but also integrates binding of receptors to scaffold molecules in the PSD.

3

A MULTISYNAPSE MODEL INTEGRATING THREE-DIMENSIONAL MORPHOLOGIES

3.1. DOMAIN OF COMPUTATION

We consider a domain that consists of a dendrite and n dendritic spines distributed along the dendrite. The dendrite is modeled as a cylinder of length l and radius R_d. As shown in Figure 3.1, the surface of the dendrite is represented as a rectangular domain $\Omega_{dendrite}$,

$$\Omega_{dendrite} := \left\{(x,y) \mid 0 < x < l\,, \quad |y| < \pi \cdot R_d\right\}. \tag{3.1}$$

The cylindrical property is preserved by imposing periodic boundary conditions on $y = \pm\pi \cdot R_d$. On this cylindrical surface dendritic spines are located. Each spine intersects the surface, such that the intersection is a closed disc Ω_j^{base} of radius R_j^{exit} around the coordinate $\boldsymbol{r}_j = (x_j, y_j)$. Its boundary is called $\partial\Omega_j$,

$$\Omega_j^{base} := \left\{\boldsymbol{r} = (x,y) \in \Omega_{dendrite} \;\middle|\; |\boldsymbol{r} - \boldsymbol{r}_j| \le R_j^{exit}\right\}, \tag{3.2}$$

$$\partial\Omega_j := \left\{\boldsymbol{r} = (x,y) \in \Omega_{dendrite} \;\middle|\; |\boldsymbol{r} - \boldsymbol{r}_j| = R_j^{exit}\right\}. \tag{3.3}$$

Furthermore, the surface of the cylinder $\Omega_{dendrite}$, excluding the discs Ω_j is denoted by Ω_0, so that

$$\Omega_0 = \Omega_{dendrite} \setminus \bigcup_{j=1}^{n} \Omega_j. \tag{3.4}$$

The domain of computation is an union of the domain Ω_0 and the dendritic spines Ω_j. The dendritic spines are modeled as out-of-plane protrusions of this surface. The morphology of these spines will be discussed in the next section.

3.1.1. MORPHOLOGY OF DENDRITIC SPINES

The dendritic spines are modeled as out-of-plane protrusions of the surface $\Omega_{dendrite}$. They intersect the dendritic surface, such that the domain of intersection is Ω_j^{base}. A receptor diffuses over the domain Ω_0 until

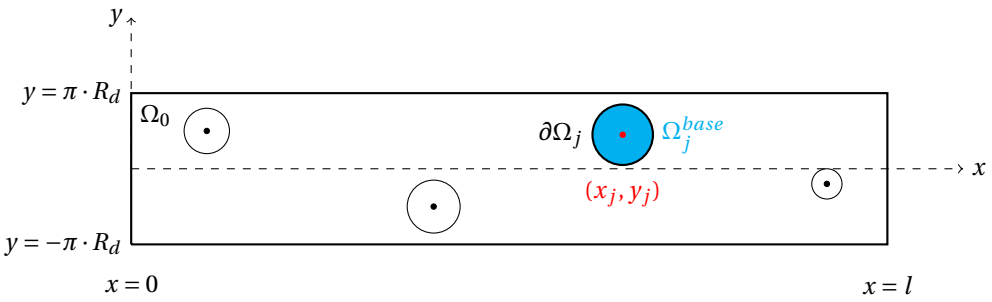

Figure 3.1: Top view of domain of computation.

it encounters the boundary of such an intersection $\partial\Omega_j$. From then on it diffuses over the surface of the respective spine Ω_j. We define this surface, using the unpublished work of Miermans, Kusters & Storm [29].

They use a Canham-Helfrich model to model the shape of membrane protrusions. This model is based on a minimum energy principle. At equilibrium, the free energy of the shape is minimized. Canham [30] proposed that the behavior of membranes is governed by minimizing the bending energy. Helfrich [31] built on this model and gave a more precise formulation.

Here, we shall give a brief explanation of the method of Miermans [29]. At $t = 0$ they define a flat membrane and fix a circle with radius 1 on it, in Figure 3.2 denoted by Γ. The surface area $\mathcal{A}$ of the membrane enclosed by this circle is in this state $\mathcal{A}_0 = \pi$. Then an iterative method is used to determine the shape of the membrane in subsequent time steps. Every time step the surface area $\mathcal{A}$ is incremented while its boundary, Γ stays fixed in plane. By minimizing the free bending energy the shape of the membrane is computed. This results in an out-of-plane deformation of the part of the domain that is within these boundaries (the blue domain in Figure 3.2). Boundary conditions are imposed on Γ to ensure smoothness of the membrane and to keep the boundary Γ at its fixed location. The solution on each time step is obtained solving a constrained minimization problem using Lagrange multipliers.

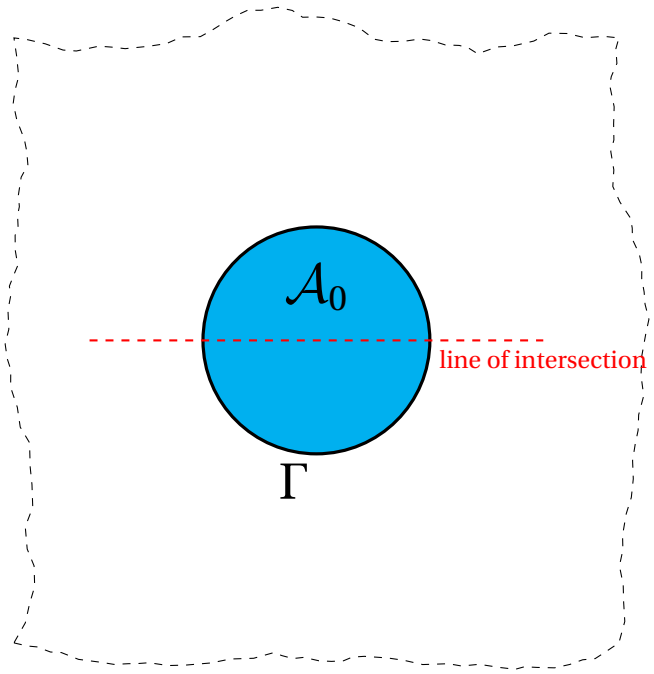

Figure 3.2: Top view of working space of Miermans et al. The blue disk, enclosed by Γ, is incrementally swollen every iteration, which results in an out-of-plane deformation (not shown here). The red line indicates the place where the intersections shown later are located.

The result of the described method are protrusions of the membrane as shown in Figure 3.3. It is these morphologies we shall use for the dendrite spines. In some cases these shapes shall be scaled for a fair comparison, however, this shall be clearly remarked when done so.

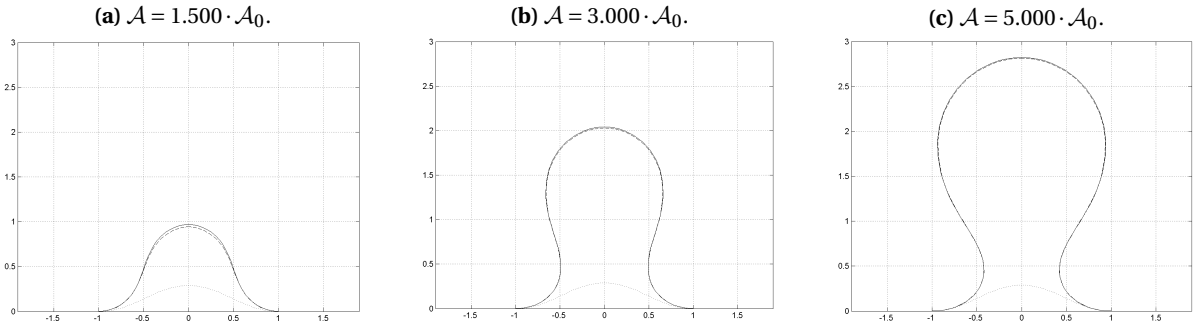

(a) $\mathcal{A} = 1.500 \cdot \mathcal{A}_0$. **(b)** $\mathcal{A} = 3.000 \cdot \mathcal{A}_0$. **(c)** $\mathcal{A} = 5.000 \cdot \mathcal{A}_0$.

Figure 3.3: Intersection of shapes for selected values of the surface area $\mathcal{A}$ as a multiple of the original surface area $\mathcal{A}_0$. Intersection is taken at the location of red dashed line in Figure 3.2. Results produced by [29].

The total domain of computation is the union of the cylindrical dendrite Ω_0, the dendritic spines Ω_j and the borders between spines and dendrite $\partial\Omega_j$ and shall be denoted by Ω,

$$\Omega = \Omega_0 \cup \bigcup_{j=1}^{n} \{\Omega_j \cup \partial\Omega_j\}. \tag{3.5}$$

3.2. DIFFUSION PROCESS

On the domain of computation Ω surface receptors are allowed to diffuse freely. Let $V(\boldsymbol{r}, t)$ denote the concentration of surface receptors within the domain of computation. The receptor surface concentration evolves according to the diffusion equation

$$\frac{\partial V}{\partial t} = D\nabla^2 V, \quad (\boldsymbol{r}, t) \in \Omega \times \mathbb{R}^+, \tag{3.6}$$

where D is the diffusion coefficient and ∇^2 denotes the Laplace-Beltrami operator.

3.2.1. BOUNDARY CONDITIONS

To preserve the cylindrical topology of the dendritic shaft, we impose periodic boundary conditions at the ends $y = \pm\pi R_d$,

$$V(x, \pi R_d, t) = V(x, -\pi R_d, t) \tag{3.7}$$

$$\frac{\partial V}{\partial y}(x, \pi R_d, t) = \frac{\partial V}{\partial y}(x, -\pi R_d, t). \tag{3.8}$$

To model zero flux at the ends $x = 0$ and $x = l$ we impose homogeneous Neumann boundary conditions

$$\frac{\partial V}{\partial x}(0, y, t) = \frac{\partial V}{\partial x}(l, y, t) = 0. \tag{3.9}$$

3.2.2. CORRESPONDING STOCHASTIC PROCESS

Our domain of computation, Ω can be seen as a two-dimensional Riemannian manifold $\mathcal{B}$ equipped with a Riemannian metric g. This metric defines a volume measure on $\mathcal{B}$, which we denote with dVol_g. The diffusion process considered here is then defined by

$$\frac{\partial \tilde{V}}{\partial t} = L\tilde{V}, \quad \text{where} \tag{3.10}$$

$$L = D\nabla_g^2. \tag{3.11}$$

Here, ∇_g^2 is the Laplace-Beltrami operator associated with the metric g. The Laplace-Beltrami operator can be expressed in the coordinates associated with the manifold $\mathcal{B}$

$$\nabla_g^2 \tilde{V} = \frac{1}{\sqrt{|\det g|}} \sum_{i,j=1}^{2} \partial_i \left(\sqrt{|\det g|} g^{ij} \partial_j \tilde{V} \right), \quad i,j = 1,2, \tag{3.12}$$

where g_{ij} are entries of the of the metric g and g^{ij} entries of the matrix inverse to the metric g. The operator L is an elliptic operator. Furthermore, Eq. (3.10) conserves the integral of $\tilde{V}$ with respect to dVol_g. The adjoint L^* of L is the generator of the stochastic process corresponding to Eq. (3.10). A review of the basics underlying the construction of diffusion on manifolds can be found in [32].

3.3. SIMULATING A STOCHASTIC PROCESS ON A CURVED SURFACE

Simulating a diffusion process on a curved surface is not trivial. Diffusion processes on manifolds are often obtained by projecting a stochastic process on a flat space onto the surface [33]. But for many anisotropic systems these methods do not work. Christensen [23] states that in such cases extreme care has to be taken, because otherwise a different diffusion operator is represented from what was initially intended.

Christensen proposes an approach to simulations of diffusive processes in general, which can also be applied to diffusion on general manfolds. He introduces a Monte Carlo type method with simulates the paths of single particles. We give a brief summary of the principles on which this method is based and an insight in our implementation. We shall focus on an application of this method to diffusion with an constant (and isotropic) diffusion tensor.

3.3.1. METHOD OF CHRISTENSEN, 2004

The method of [23] is based on the observation that every Monte Carlo update scheme moving a particle from $\boldsymbol{r}_0$ to $\boldsymbol{r}$ in a time interval Δt prescribes a certain transition rate and that a correct numerical method matches the first and second moments of this transition rate to the ones of the original diffusion equation.

The method of Christensen starts of with an equation describing the development of a particles probability distribution P, with constant and scalar diffusion tensor D

$$\frac{\partial P}{\partial t} = D\nabla^2 P. \tag{3.13}$$

Then an update routine is constructed, involving two spatial and two temporal components specified in Table 3.1. $f(\xi)$ and l together represent the radial jump distribution in the physical space and $h(\zeta)$ and τ represent the distribution of waiting times between successive jumps.

Component	Description
$f(\xi)$	dimensionless radial distribution
$l > 0$	typical jump length
$h(\zeta) > 0$	dimensionless temporal distribution
$\tau > 0$	time scale

Table 3.1: Components representing jump distribution in physical space and waiting times between jumps of method proposed by Christensen [23].

The moments of $f(\xi)$ and $h(\zeta)$ are denoted by $\overline{\xi^m}$ and $\overline{\zeta^m}$ respectively. Furthermore, the dimensionless (scalar) diffusion tensor $b = D\overline{\zeta}\tau/\overline{\xi^2}l^2$ is introduced. Now, we provide the update mechanism that implements the simulation of a moving particle from a starting position $(\boldsymbol{r}, t)$ to $(\boldsymbol{r}+\Delta\boldsymbol{r}, t+\Delta t)$ in an n-dimensional environment. The procedure is given in Alg. 1.

Algorithm 1 Algorithm as presented by [23].

Initialization: Calculate $b = D\overline{\zeta}\tau/\overline{\xi^2}l^2$.

1: Draw a dimensionless waiting time ζ from distribution h and set $\Delta t = \zeta\tau/(2n)$.
2: Choose a test step $\Delta\boldsymbol{r}$:
   a. Choose a unit vector $\boldsymbol{w}$ from a uniform distribution over all directions.
   b. Choose a dimensionless, radial jump length ξ from distribution f.
   c. Calculate $\Delta\boldsymbol{r}$ by moving a length $|\sqrt{b}\boldsymbol{w}|\xi l$ along a geodesic in the direction of $\boldsymbol{w}$.
3: Update $(\boldsymbol{r}, t) \longrightarrow (\boldsymbol{r}+\Delta\boldsymbol{r}, t+\Delta t)$.

Analytic solutions of a geodesic are not generally found. However, if the jump length is small enough, good approximations can be easily obtained using a Taylor expansion.

3.3.2. SIMPLIFICATIONS AND IMPLEMENTATION

Simplifications to the scheme of [23] are possible. Christensen recommends to use fixed steps in space and time, because any couple of distributions f and h will do if l is small enough. We adopt this recommendation and fix a spacial step size λ. Furthermore, since we consider diffusion on a surface we fix the dimension $n = 2$. Alg. 1 then reduces to Alg. 2.

Algorithm 2 Algorithm as presented by [23], adapted to a fixed spacial step size λ.

Initialization:
   Fix a spacial step size $\lambda > 0$.
   Set $\Delta t = \lambda^2/4D$.

1: Choose a test step $\Delta\boldsymbol{r}$:
   a. Choose a unit vector $\boldsymbol{w}$ from a uniform distribution over all directions.
   b. Calculate $\Delta\boldsymbol{r}$ by moving a length λ along a geodesic in the direction of $\boldsymbol{w}$.
2: Update $(\boldsymbol{r}, t) \longrightarrow (\boldsymbol{r}+\Delta\boldsymbol{r}, t+\Delta t)$.

A geodesic curve parametrized by arch length s can be approximated in the same way [22] did, as given in Eq. (2.6). The Taylor expansion used is

$$\boldsymbol{r}(s+\mathrm{d}s) = \boldsymbol{r}(s) + \frac{\mathrm{d}\boldsymbol{r}(s)}{\mathrm{d}s}\mathrm{d}s + \frac{1}{2}\frac{\mathrm{d}^2\boldsymbol{r}(s)}{\mathrm{d}s^2}\mathrm{d}s^2 + \mathcal{O}(\mathrm{d}s^3). \tag{3.14}$$

If the spatial step size λ is small enough, leaving out the $\mathcal{O}(\mathrm{d}s^3)$-term in Eq. (3.14) constitutes a good approximation. The second order terms can be calculated as in Eq. (2.7). The resulting updating scheme for the positions is then given by Eqs. (2.8, 2.9).

3.3.3. DEALING WITH BOUNDARY CONDITIONS

An additional advantage of this implementation is that boundary conditions like reflection, absorption or a mixture of the two are easily implemented. Since the paths single particles are simulated we can apply the boundary conditions per individual particle. If a particle encounters a reflecting boundary, geometrical rules of reflection can be applied. If a particle encounters an absorbing boundary, it is taken out of the system.

4

FIRST RESULTS

Is this Chapter we shall present the results of the first test cases that were implemented. The test cases have a similar design. A dendrite of certain length and radius is introduced with two spines attached to it. The geometry of the two spines is identical per test case, but different for each distinct test case.

4.1. DESIGN OF THE TEST CASES

The geometry of the test cases is schematically shown in Figure 4.1. We define a working space of length L and width $w = 2\pi \cdot R_d$, where R_d denotes the radius of the dendrite. We have reflection conditions at $x = 0$ and $x = L$ and periodic boundary conditions at $y = \pm\pi \cdot R_d$.

This area is populated by two circular geometries modeling the entry of two spines. The centers of these circles are spaced at a distance of a in the x-direction and the radius is denoted by R_{exit}.

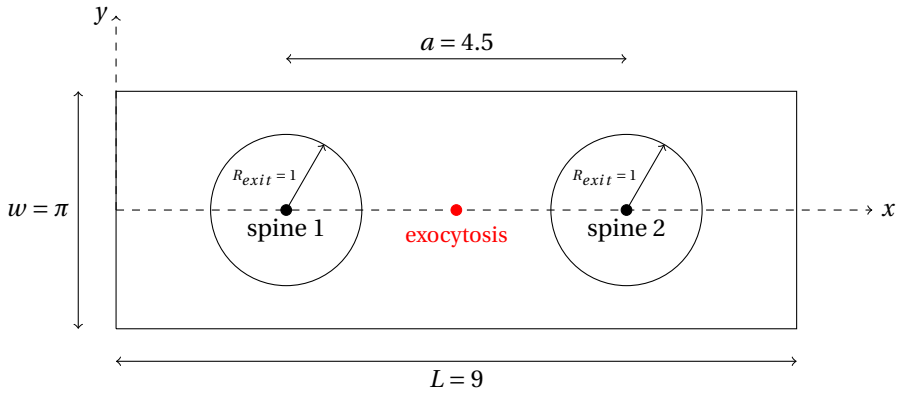

Figure 4.1: Top view of geometry of test cases, all units μm. Red dot indicates dendritic exocytosis in the middle between the two spines.

For the morphology of the spines we use the results of [29], as discussed in Section 3.1.1. We use three different morphologies, corresponding to a surface area of $A = 1.5$, 3.0 and 5.0. The radii of these spines can be found in Figure 4.2. Because the spines are axially symmetric, these radii completely define the geometry of the spines.

The post synaptic density is modeled by an absorbing boundary at the top of each spine. This absorbing boundary is chosen to be a circle with radius R_{PSD}.

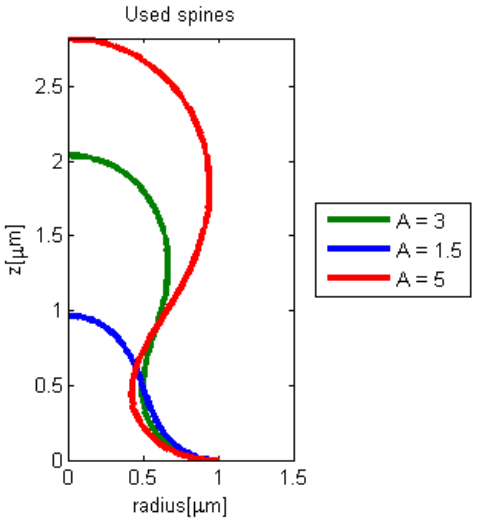

Figure 4.2: Radii of used spines. *A* indicates the factor the surface area of the spine has swollen.

The parameters used are:

$$\begin{aligned} L &= 9, \\ R_{dendrite} &= 0.5, \\ a &= 4.5, \\ R_{exit} &= 1, \\ R_{PSD} &= 0.2. \end{aligned} \tag{4.1}$$

An exocytic event of 5000 particles is simulated for each test case. To begin with, the exocytosis is located in the middle between the two spines, as indicated in red in Figure 4.1.

After simulating the exocytic event, simulations were run until all particles left the system through either the absorbing boundary (modeling the PSD) in spine 1 or spine 2. The place of departure of the system and the corresponding exit time were recorded.

4.2. RESULTS

The described procedure constitutes a Monte Carlo simulation. After the simulation is done, each particle released at the exocytosis serves as a realization in the Monte Carlo method. Per realization the exit location (the absorbing boundary in either spine 1 or spine 2) and the exit time are recorded. From the results of this simulation sample mean and sample standard deviations can be calculated, including there respective confidence intervals. The overall MFPT is denoted with μ_{FPT} and its (unbiased) estimator, the sample mean with $\hat{\mu}_{FPT}$. The standard deviation of the MFPT is denoted with σ_{FPT} and its (unbiased) estimator, the sample standard deviation, with $\hat{\sigma}_{FPT}$. A similar and intuitive notation is used for the specific boundaries:

μ^i_{FPT}	MFPT of particles exiting from spine i;
$\hat{\mu}^i_{FPT}$	corresponding sample mean;
σ^i_{FPT}	standard deviation of MFPT of particles exiting from spine i;
$\hat{\sigma}^i_{FPT}$	corresponding sample standard deviation.

4.2.1. DENDRITIC EXOCYTOSIS IN THE MIDDLE BETWEEN TWO SPINES

First we compare the different shapes by simulating an exocytic event in the middle of the two spines. These test cases are symmetric and the MFPT at spine 1 is (statistically) the same as the MFPT at spine 2. An estimate for the MFPT and its standard deviation are given in Table 4.1. We also present 95% confidence intervals.

Shape parameter	$\hat{\mu}_{FPT}[s]$		$\hat{\sigma}_{FPT}[s]$	[95% conf.]
$A = 1.5$	75	± 1.8	66.3	[65.0, 67.6]
$A = 3.5$	144	± 3.6	128.6	[126.1, 131.2]
$A = 5.0$	199	± 4.7	171.1	[167.8, 174.5]

Table 4.1: Sample mean and sample deviation of first passage times for dendritic exocytosis of 5.000 particles in the middle between two spines as a function of the morphology of the spines. The intervals given are 95% confidence intervals.

The results of these simulations can also be shown as empirical probability distribution functions. These are plotted in Figure 4.3.

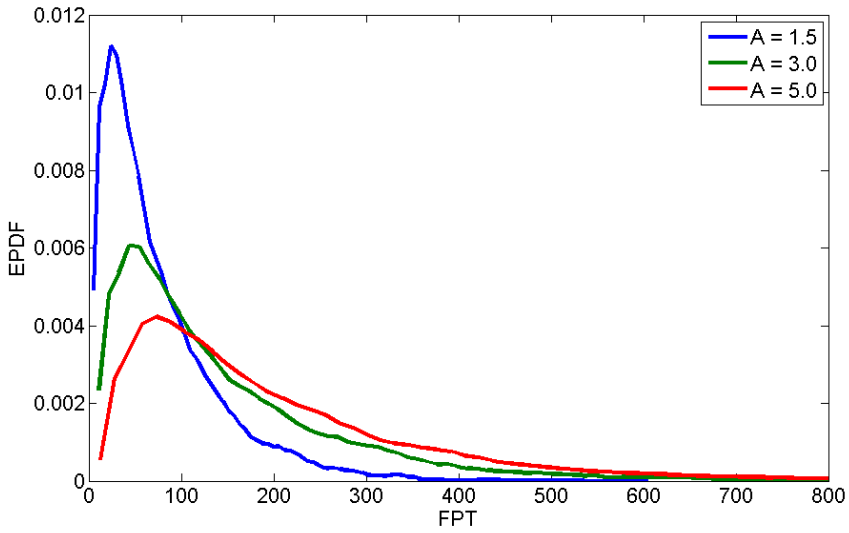

Figure 4.3: Empirical probability distribution functions for an exocytic event in the middle between two spines of identical morphology. Simulation performed for three values of A.

4.2.2. SPINAL EXOCYTOSIS IN ONE SPINE

Next, we simulate an exocytic event in one of the two spines. The geometry of the domain stays otherwise the same.

Since the surface area nor the height of the spines are equal among the shapes we investigate (Fig. 4.2), there is no straightforward exocytosis location that allows us to make a meaningful comparison. We chose to define the location of exocytosis at that point at which there is as much surface area between the absorbing boundary modeling the PSD and the boundary coupling the spine to the dendrite. There are many other options for this choice, for example equating the shortest distance between the chosen location and the PSD and the chosen location and the boundary between spine and dendrite. All options have their own considerations, but a choice has to be made.

Since the problem is nonsymmetric, we shall present results for the two spines separately. For particles exiting the system through the same spine in which the exocytosis took place we shall make a distinction between particles first leaving this spine to the dendrite before returning and particles that hit the absorbing boundary at the PSD before leaving to the dendrite. This last class of particles shall be denoted with *indirect absorption*.

SAMPLE MEAN, SAMPLE STANDARD DEVIATION AND OTHER EXIT STATISTICS

In Table 4.2-4.4 the exit statistics for the three test are presented. For shape parameters $A = 1.5$ and $A = 3.0$ 81% of the particles exit the system through the spine in which they originate at exocytosis. For $A = 5.0$ this is slightly more, 85%. We can conclude that in this experiment the shape belonging to $A = 5.0$ (Fig. 4.2) allows the synapse to be controlled more specifically with spinal exocytosis then the other shape parameters.

$A = 1.5$	$\hat{\mu}_{FPT}[s]$		$\hat{\sigma}_{FPT}[s]$		Exit %
Overall	50.8	±1.8	63.9	[62.6, 65.2]	5000 (100%)
Spine 1	39.6	±1.8	57.9	[56.6, 59.2]	4049 (81 %)
Spine 1, direct	2.7	±0.2	2.0	[1.9, 2.2]	1150 (23%)
Spine 1, indirect	54.3	±1.2	62.6	[61.0, 64.3]	2899 (58%)
Spine 2	98.3	±4.2	66.5	[63.6, 69.7]	951 (19%)

Table 4.2: Sample mean and sample deviation of first passage times for spinal exocytosis of 5.000 particles in spine 1, with shape parameter $A = 1.5$. The intervals given are 95% confidence intervals.

$A = 3.0$	$\hat{\mu}_{FPT}[s]$		$\hat{\sigma}_{FPT}[s]$		Exit %
Overall	83.3	±3.2	113.7	[111.5, 116.0]	5000 (100%)
Spine 1	61.9	±3.1	100.3	[98.1, 102.5]	4117 (81 %)
Spine 1, direct	9.8	±0.3	7.7	[7.4, 7.9]	2130 (43%)
Spine 1, indirect	117.9	±5.4	121.4	[117.7, 125.2]	1987 (40%)
Spine 2	182.9	±7.9	119.7	[114.3, 125, 6]	883 (18%)

Table 4.3: Sample mean and sample deviation of first passage times for spinal exocytosis of 5.000 particles in spine 1, with shape parameter $A = 3.0$. The intervals given are 95% confidence intervals.

	$\hat{\mu}_{FPT}[s]$		$\hat{\sigma}_{FPT}[s]$		Exit %
Overall	108.1	±4.1	148.9	[146.0, 151.9]	5000 (100%)
Spine 1	82.8	±3.9	131.0	[128.3, 133.8]	4260 (85%)
Spine 1, direct	22.5	±0.7	19.9	[19.4, 20.4]	2740 (55%)
Spine 1, indirect	191.5	±8.6	170.3	[164.5, 176.6]	1520 (30%)
Spine 2	253.6	±11.7	162.2	[154.3, 170.9]	740 (15%)

Table 4.4: Sample mean and sample deviation of first passage times for spinal exocytosis of 5.000 particles in spine 1. The intervals given are 95% confidence intervals.

In Fig. 4.4-4.6 the empirical probability distribution functions can be found. The particles are sorted based on their exit location (spine 1 or spine 2) . Also, for the particles leaving the system through the absorbing boundary in spine 1 a distinction is made when particles leave the spine to the dendrite prior to returning and leaving the system through spine 1. These particles are referred to with *indirect* and the corresponding EPDF can also be found in Fig. 4.4-4.6.

From these figures we can see that the distributions qualitatively look the same for each test case , but the time scales are different. The time scales increase when A increases. This might not only be due to shape, but also because the domain of computation consists of a greater area.

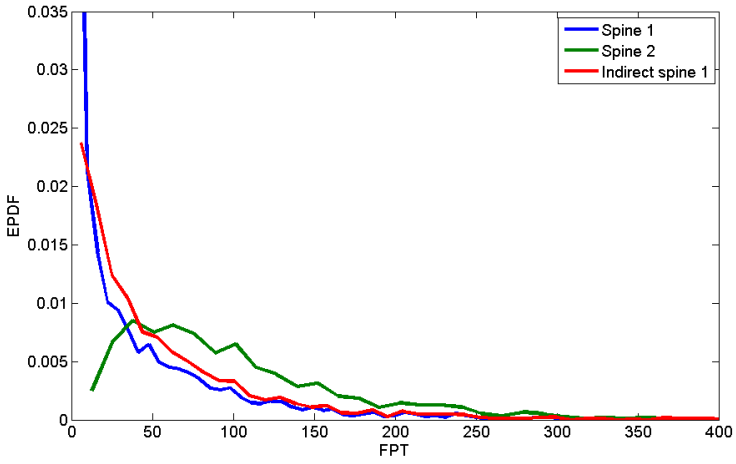

Figure 4.4: Empirical probability distribution functions for a spinal exocytic event in spine 1, with shape parameter $A = 1.5$.

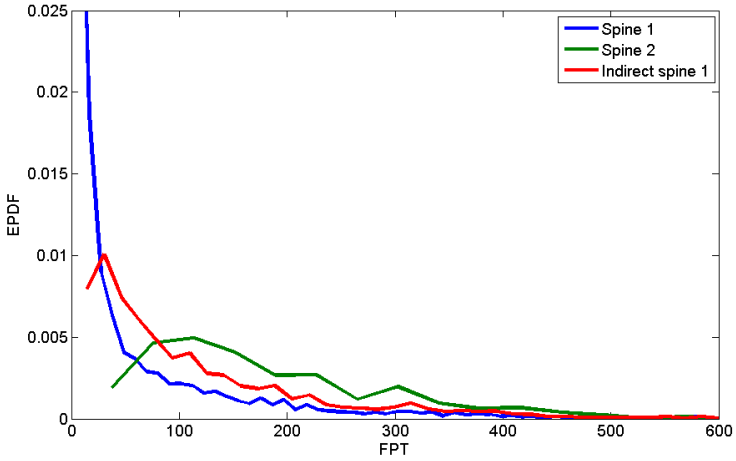

Figure 4.5: Empirical probability distribution functions for a spinal exocytic event in spine 1, with shape parameter $A = 3.0$.

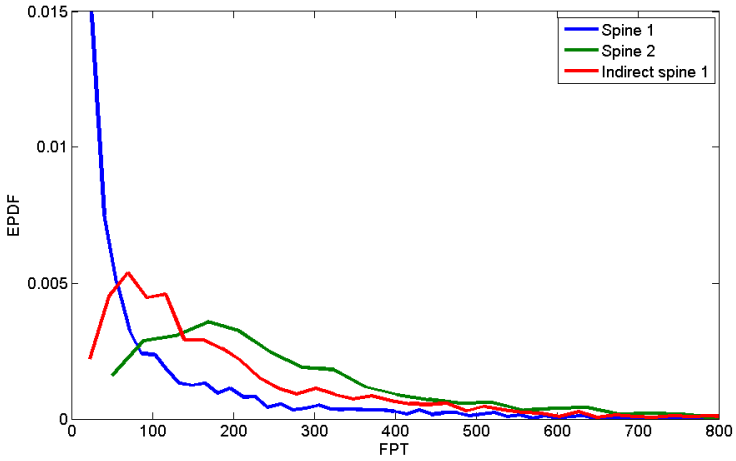

Figure 4.6: Empirical probability distribution functions for a spinal exocytic event in spine 1, with shape parameter $A = 5.0$.

BIBLIOGRAPHY

[1] T. C. Sudhof, *The synaptic vesicle cycle,* Annual Review of Neuroscience **27**, 509 (2004).

[2] M. Sheng and C. C. Hoogenraad, *The postsynaptic architecture of excitatory synapses: a more quantitative view,* Annual Review of Biochemistry **76**, 823 (2007).

[3] R. M. Julien, *A primer of drug action: A concise, nontechnical guide to the actions, uses, and side effects of psychoactive drugs* (WH Freeman, Times Books, Henry Holt & Co, 1995).

[4] H. Kasai, M. Matsuzaki, J. Noguchi, N. Yasumatsu, and H. Nakahara, *Structure–stability–function relationships of dendritic spines,* Trends in Neurosciences **26**, 360 (2003).

[5] J. I. Arellano, R. Benavides-Piccione, J. DeFelipe, and R. Yuste, *Ultrastructure of dendritic spines: correlation between synaptic and spine morphologies,* Frontiers in Neuroscience **1**, 131 (2007).

[6] T. Tada and M. Sheng, *Molecular mechanisms of dendritic spine morphogenesis,* Current Opinion in Neurobiology **16**, 95 (2006).

[7] I. M. Ethell and E. B. Pasquale, *Molecular mechanisms of dendritic spine development and remodeling,* Progress in Neurobiology **75**, 161 (2005).

[8] J. Tønnesen, G. Katona, B. Rózsa, and U. V. Nägerl, *Spine neck plasticity regulates compartmentalization of synapses,* Nature neuroscience **17**, 678 (2014).

[9] M. Adrian, R. Kusters, C. J. Wierenga, C. Storm, C. C. Hoogenraad, and L. C. Kapitein, *Barriers in the brain: resolving dendritic spine morphology and compartmentalization,* Frontiers in Neuroanatomy **8**, 142 (2014).

[10] D. C. Javitt, *Glutamate as a therapeutic target in psychiatric disorders,* Molecular Psychiatry **9**, 984 (2004).

[11] G. Dawson, *Early behavioral intervention, brain plasticity, and the prevention of autism spectrum disorder,* Development and Psychopathology **20**, 775 (2008).

[12] B. B. Johansson, *Brain plasticity and stroke rehabilitation: The Willis lecture,* Stroke **31**, 223 (2000).

[13] K. Gerrow and A. Triller, *Synaptic stability and plasticity in a floating world,* Current Opinion in Neurobiology **20**, 631 (2010).

[14] J.-L. Gaiarsa, O. Caillard, and Y. Ben-Ari, *Long-term plasticity at gabaergic and glycinergic synapses: mechanisms and functional significance,* Trends in Neurosciences **25**, 564 (2002).

[15] T. V. Bliss and G. L. Collingridge, *A synaptic model of memory: long-term potentiation in the hippocampus,* Nature **361**, 31 (1993).

[16] V. A. Derkach, M. C. Oh, E. S. Guire, and T. R. Soderling, *Regulatory mechanisms of AMPA receptors in synaptic plasticity,* Nature Reviews Neuroscience **8**, 101 (2007).

[17] R. Yuste and T. Bonhoeffer, *Morphological changes in dendritic spines associated with long-term synaptic plasticity,* Annual review of neuroscience **24**, 1071 (2001).

[18] D. Meyer, T. Bonhoeffer, and V. Scheuss, *Balance and stability of synaptic structures during synaptic plasticity,* Neuron **82**, 430 (2014).

[19] D. Holcman and Z. Schuss, *Diffusion laws in dendritic spines,* The Journal of Mathematical Neuroscience **1**, 10 (2011).

[20] Z. Schuss, *Theory and applications of stochastic processes: an analytical approach*, Vol. 170 (Springer Science & Business Media, 2009).

[21] R. Kusters, L. C. Kapitein, C. C. Hoogenraad, and C. Storm, *Shape-induced asymmetric diffusion in dendritic spines allows efficient synaptic AMPA receptor trapping,* Biophysical Journal **105**, 2743 (2013).

[22] R. Kusters and C. Storm, *Impact of morphology on diffusive dynamics on curved surfaces,* Physical Review E **89** (2014), 10.1103/PhysRevE.89.032723.

[23] M. Christensen, *How to simulate anisotropic diffusion processes on curved surfaces,* Journal of Computational Physics **201**, 421 (2004).

[24] K. Czöndör, M. Mondin, M. Garcia, M. Heine, R. Frischknecht, D. Choquet, J.-B. Sibarita, and O. R. Thoumine, *Unified quantitative model of AMPA receptor trafficking at synapses,* Proceedings of the National Academy of Sciences **109**, 3522 (2012).

[25] P. C. Bressloff, B. A. Earnshaw, and M. J. Ward, *Diffusion of protein receptors on a cylindrical dendritic membrane with partially absorbing traps,* SIAM Journal on Applied Mathematics **68**, 1223 (2008).

[26] B. A. Earnshaw and P. C. Bressloff, *Biophysical model of AMPA receptor trafficking and its regulation during long-term potentiation/long-term depression,* Journal of Neuroscience **26**, 12362 (2006).

[27] D. Holcman and A. Triller, *Modeling synaptic dynamics driven by receptor lateral diffusion,* Biophysical Journal **91**, 2405 (2006).

[28] B. A. Earnshaw and P. C. Bressloff, *Modeling the role of lateral membrane diffusion in AMPA receptor trafficking along a spiny dendrite,* Journal of Computational Neuroscience **25**, 366 (2008).

[29] K. Miermans, R. Kusters, and C. Storm, *On the morphology of dendritic spines,* (2015), part of master thesis at TU Eindhoven.

[30] P. B. Canham, *The minimum energy of bending as a possible explanation of the biconcave shape of the human red blood cell,* Journal of Theoretical Biology **26**, 61 (1970).

[31] W. Helfrich, *Elastic properties of lipid bilayers: theory and possible experiments,* Zeitschrift für Naturforschung C **28**, 693 (1973).

[32] F. Debbasch and C. Chevalier, *Diffusion processes on manifolds,* in *Markov Processes and Related Topics: A Festschrift for Thomas G. Kurtz*, Collections, Vol. 4, edited by S. N. Ethier, J. Feng, and R. H. Stockbridge (Institute of Mathematical Statistics, Beachwood, Ohio, USA, 2008) pp. 85–97.

[33] N. Ikeda and S. Watanabe, *Stochastic differential equations and diffusion processes* (North-Holland/Kodansha, 1989).